Dynamic and Thermodynamic Response of the Ras Protein Cdc42Hs upon Association with the Effector Domain of PAK3

ARTICLE *in* JOURNAL OF MOLECULAR BIOLOGY · AUGUST 2014

Impact Factor: 4.33 · DOI: 10.1016/j.jmb.2014.07.031 · Source: PubMed

7 AUTHORS, INCLUDING:

Veronica R Moorman
Kettering University
10 PUBLICATIONS **78** CITATIONS
SEE PROFILE

Vignesh Kasinath
University of Pennsylvania
11 PUBLICATIONS **110** CITATIONS
SEE PROFILE

Andrew Joshua Wand
University of Pennsylvania
193 PUBLICATIONS **8,712** CITATIONS
SEE PROFILE

Dynamic and Thermodynamic Response of the Ras Protein Cdc42Hs upon Association with the Effector Domain of PAK3

Veronica R. Moorman, Kathleen G. Valentine, Sabrina Bédard, Vignesh Kasinath, Jakob Dogan, Fiona M. Love and A. Joshua Wand

Graduate Group in Biochemistry and Molecular Biophysics, *Johnson Research Foundation and Department of Biochemistry and Biophysics, Perelman School of Medicine, University of Pennsylvania, Philadelphia, PA 19104–6059, USA*

Correspondence to A. Joshua Wand: *Department of Biochemistry and Biophysics, Perelman School of Medicine, University of Pennsylvania, 905 Stellar-Chance Laboratories, 422 Curie Boulevard, Philadelphia, PA 19104–6059, USA.*
wand@mail.med.upenn.edu
http://dx.doi.org/10.1016/j.jmb.2014.07.031
Edited by C. Kalodimos

Abstract

Human cell division cycle protein 42 (Cdc42Hs) is a small, Rho-type guanosine triphosphatase involved in multiple cellular processes through its interactions with downstream effectors. The binding domain of one such effector, the actin cytoskeleton-regulating p21-activated kinase 3, is known as PBD46. Nitrogen-15 backbone and carbon-13 methyl NMR relaxation was measured to investigate the dynamical changes in activated GMPPCP·Cdc42Hs upon PBD46 binding. Changes in internal motion of the Cdc42Hs, as revealed by methyl axis order parameters, were observed not only near the Cdc42Hs–PBD46 interface but also in remote sites on the Cdc42Hs molecule. The binding-induced changes in side-chain dynamics propagate along the long axis of Cdc42Hs away from the site of PBD46 binding with sharp distance dependence. Overall, the binding of the PBD46 effector domain on the dynamics of methyl-bearing side chains of Cdc42Hs results in a modest rigidification, which is estimated to correspond to an unfavorable change in conformational entropy of approximately −10 kcal mol^{-1} at 298 K. A cluster of methyl probes closest to the nucleotide-binding pocket of Cdc42Hs becomes more rigid upon binding of PBD46 and is proposed to slow the catalytic hydrolysis of the γ phosphate moiety. An additional cluster of methyl probes surrounding the guanine ring becomes more flexible on binding of PBD46, presumably facilitating nucleotide exchange mediated by a guanosine exchange factor. In addition, the Rho insert helix, which is located at a site remote from the PBD46 binding interface, shows a significant dynamic response to PBD46 binding.

Introduction

Human cell division cycle homolog protein 42 (Cdc42Hs)* is a member of the Ras family of small guanosine triphosphatases (GTPases). Interactions with various proteins allow the Rho GTPases to be highly coordinated “molecular switches”. Activated Cdc42Hs regulates a variety of cellular responses, principally involving actin polymerization, intracellular trafficking and cell growth regulation, through interactions with multiple downstream effector proteins [1]. Through their regulatory interactions with guanine nucleotide exchange factors (GEFs), GTPase-activating proteins (GAPs) and guanine nucleotide dissociation inhibitors (GDIs), GTPases cycle between an activated, guanosine triphosphate (GTP)-bound state and an inactive, guanosine diphosphate (GDP)-bound state [2,3].

All members of the Rho subfamily of GTPases share a common fold consisting of five α-helices, a central β-sheet and a conserved nucleotide-binding pocket [4]. Activation of members of this family results in a structural response, mainly in two regions of the protein, termed Switches I and II, that are central to GTP hydrolysis and binding of downstream effector proteins [5]. Many of the effector proteins bind the active, GTP-bound form of Cdc42Hs via a Cdc42/Rac interactive binding (CRIB) motif that binds between the two switch regions of Cdc42Hs and forms an additional strand to the central β-sheet. One such

CRIB-containing effector protein family is the actin cytoskeleton-regulating p21-activated serine/threonine kinase 3 (PAK3) family. Members of this family are implicated in numerous human diseases [6–8] and are some of the most thoroughly studied effectors of Cdc42Hs [9].

The GTP-activated state of Cdc42Hs initiates cellular signaling cascades via PAK3 kinase CRIB-binding domain, which inhibits the GTPase activity of Cdc42Hs [10]. A significant structural feature of the Rho family members is the presence of an α-helix containing the so-called Rho insert region [11]. This helix has been implicated in the intracellular signaling of the membrane associated activated GTPase. The signaling is proposed to initiate in response to a reorientation of the Rho insert helix with the subsequent activation of the GDI, an effector protein of the Rho GTPases [12,13]. Important structural features of Cdc42Hs are highlighted in Fig. 1. The structural response of the activated GTPase Cdc42Hs to binding the downstream PAK3 effector PBD46 is localized to the binding interface [14,15]. The ensuing cascade of molecular events requires a more distal response than the structural changes might suggest. The dynamical response of activated Cdc42Hs to effector binding Cdc42Hs is the focus of this study.

The association of proteins with ligands is a central aspect of biochemical work and has a complex thermodynamic origin [16,17]. A fundamental consideration of the thermodynamics of ligand binding is the potential contribution from changes in protein conformational entropy and has generated much discussion and speculation over the past few decades [18–22]. It is only recently that experimental methods and analytical strategies have emerged to allow determination of changes in protein conformational entropy upon a change in functional state and use of comprehensive measures of changes in internal protein motion as a "dynamical proxy" for the conformational entropy that they reflect [23–26].

The first experimental demonstration of large-scale changes in internal protein motion due to the binding of a ligand to a protein examined the interaction of calcium-activated calmodulin with peptides corresponding to calmodulin-binding domains of regulated proteins [27]. With the use of a simple model-dependent "oscillator inventory" interpretation [28], the changes in the fast motion (nanosecond-to-picosecond timescale) of the methyl-bearing side chains of calmodulin suggested that changes in the conformational entropy of calmodulin were on the order of the free energy of binding [27]. Subsequently, a linear correlation between the total entropy of binding and the apparent conformational entropy was observed across a family of calmodulin complexes, suggesting that evolution has employed the variation in conformational entropy to adjust the free energy of binding [24]. More recently, it has become clear that changes in NMR-derived order parameters can indeed be used as a quantitative proxy for conformational entropy and may be generally useful as an "entropy meter" [25,26]. Molecular dynamics simulations also suggest that the linear relationship between the order parameter and the calculated rotamer entropy of the methyl-bearing side chains has simple physical origins [26].

Whether large contributions to the free energy of formation of protein–protein complexes by changes in conformational entropy are pervasive remains an

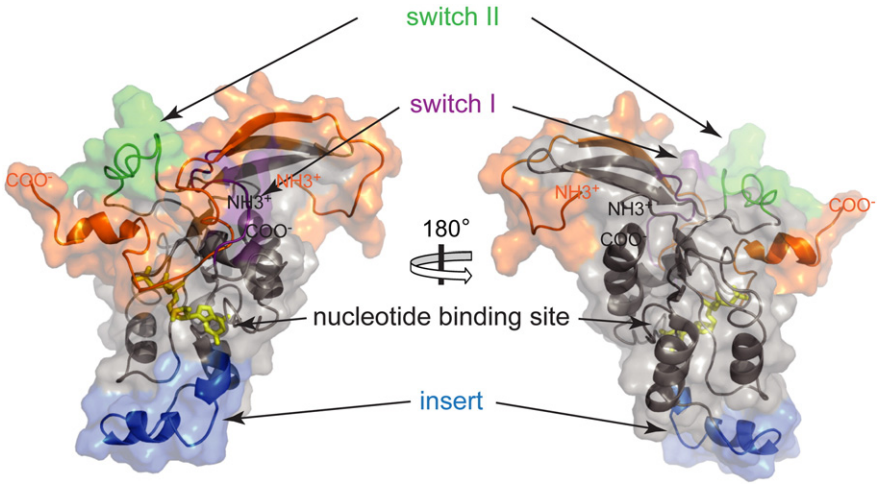

Fig. 1. Views of the structure of Cdc42Hs·GMPPCP bound to PBD46 [14] (PDB ID: 1EES). Cdc42Hs is depicted with gray ribbons and PBD46 is depicted in orange ribbons; the surface of the complex is colored as the protein or peptide. Three regions of interest in the Cdc42Hs protein are designated by colors. Switch I [55] is in purple, Switch II [55] is in green and the Rho insert region [5] is in blue. The GTP analog (GMPPCP) shown in yellow is absent from the deposited model owing to insufficient structural restraints [14] and was therefore modeled here using a homologous binary complex [54] (PDB ID: 2QRZ). Structural renderings in this and subsequent figures were generated using the program PyMOL [89].

important question. A central feature of calmodulin is its promiscuity toward binding partners [29] and suggests that conformational entropy offers a means to maintain optimal binding free energies while solving the molecular recognition problem presented by a large family of interacting ligands. The Rho GTPase proteins represent an important superfamily that is also centrally engaged in protein-mediated signal transduction pathways in eukaryotes [30] and it is of interest to determine whether they also employ dynamically modulated responses to ligand binding.

The structural and dynamic aspects of the interaction of Cdc42Hs with the binding domain of the PAK3 kinase (PBD46) have been previously studied by solution NMR methods [14,31,32]. With the use of deuterium relaxation methods, significant changes in the dynamics of methyl-bearing side chains were apparently observed upon binding of the PBD46 domain to the binary complex of Cdc42Hs with a non-hydrolyzable GTP analog, GMPPCP [32]. The total entropy of binding as determined by isothermal titration calorimetry (ITC) is unfavorable [32], yet changes in methyl side-chain motion were both large and widely distributed and were interpreted as corresponding to a net increase (favorable) change in conformational entropy of Cdc42Hs upon binding the PBD46 domain. That study represented the first site-resolved experimental indication of the entropy-driven allosteric response envisaged by Cooper and Dryden over 15 years earlier [19]. Unfortunately, as discussed below, the deuterium relaxation experiments employed are somewhat ill-suited for a protein complex of this size (24 kDa). Since then, carbon relaxation methods that provide more accurate information about side-chain motion in large protein systems have been introduced [33,34]. Here we undertake carbon relaxation measurements to revisit the interaction of the activated Cdc42Hs (bound to the GTP analog GMPPCP) with the PBD46 domain. Our results contradict the previous deuterium relaxation study and lead to decidedly different conclusions. The data presented here document an overall decrease in conformational entropy on binding of the PBD46 domain to the Cdc42Hs (entropically unfavorable). The site-specific dynamical changes noted in this study are interpreted in terms of the functional aspects required of the cascade of protein–protein interactions in response to the binding of the PAK domain to the Cdc42Hs Ras protein.

Results and Discussion

Resonance assignments

With the use of standard triple resonance and total correlation (TOCSY) experiments, side-chain methyl and backbone amide chemical shifts were assigned for both the Cdc42Hs·GMPPCP binary and the Cdc42Hs·GMPPCP–PBD46 ternary complexes. Previously reported assignments of the Cdc42Hs·GMPPCP complex [5] were largely confirmed and significantly extended to include 103 of the 120 methyl groups in the Cdc42Hs protein. Monitoring the titration of Cdc42Hs·GMPPCP with PBD46 by ^{15}N-heteronuclear single quantum coherence (HSQC) experiments confirms that binding is in slow exchange on the NMR chemical shift timescale [35]. Assignments corresponding to the ternary complex were not available and were thus obtained *de novo*. With the use of samples over-titrated with the PBD46 peptide ligand to suppress chemical exchange effects, 92 methyl resonance assignments were made. Importantly, the assignments of amide ^{15}N-^{1}H and methyl ^{13}C-^{1}H correlations included pairwise sets from 105 backbone residues and 79 methyl sites, which is a significant advantage for the subsequent analysis of conformational entropy (see below). The chemical shifts are compiled in Tables S1 and S2 and are summarized in Table S3. They have been also deposited to the Biological Magnetic Resonance Bank (BMRB) under accession numbers 18251 and 18252.

Characterization of macromolecular tumbling and motion of the backbone

Backbone amide T_1, T_2 and nuclear Overhauser enhancement (NOE) relaxation parameters at 14.1 and 17.6 T were measured using standard experiments [36] and were used to characterize the overall macromolecular tumbling models and to obtain the Lipari–Szabo squared generalized order parameter (O^2_{NH}) [37]. In the binary state (Cdc42Hs·GMPPCP), 128 N–H probes were sufficiently resolved for analysis. Forty-eight probe sites were excluded from the molecular tumbling fitting routine if they met at least one of the following three criteria: ^{1}H-^{15}N NOE values less than 0.6, the product of the T_1 and the T_2 greater than 1.5 or the fit of the τ_m, τ_e and O^2_{NH} produce statistical outliers to the normalized χ^2 values. The remaining 80 probes were used to determine the macromolecular tumbling characteristics of Cdc42Hs·GMPPCP. Comparisons among purely isotropic [37], axially symmetric and fully anisotropic [38] tumbling models established that the binary complex fits best to an axially symmetric tumbling model with a molecular correlation time of 12.3 ± 0.1 ns and the ratio of the diffusion tensor elements $D_{\parallel}/D_{\perp}$ equal to 1.086 (Table 1). Final model-free and R_{ex} parameters for each site were obtained by local fitting of the 128 N–H probes with the determined axially symmetric tumbling parameters. Thirty-eight of these sites then showed statistically significant R_{ex}. As is generally the case for well-structured proteins [23,39], the backbone ^{15}N–^{1}H squared generalized order parameters (O^2_{NH}) of the

Table 1. Characterization of macromolecular tumbling of the binary (Cdc42Hs·GMPPCP) and ternary (Cdc42Hs·GMPPCP·PBD46) complexes of Cdc42Hs

	Number of probes	F_x (anisotropic)[a]	F_x (axially symmetric)[a]	Best model ($D_\parallel/D_\perp$)[b]	Isotropic τ_m (ns)[c]
Binary complex	90	11.3	14.7	Axially symmetric (1.086)	12.3 ± 0.1 (14.9 ± 0.1)
Ternary complex	101	0.1	−3.1	Isotropic	16.7 ± 0.1

[a] F_x values to determine the most appropriate tumbling model are defined by Eq. (1). Both models are compared with the completely isotropic model. Negative values indicate that the more complex model is not statistically warranted.
[b] Value in parenthesis indicates the anisotropic ratio of the diffusion tensor elements, parallel with the principle axis over perpendicular.
[c] Values in parentheses are corrected for the increased viscosity due to the added amount of D_2O in the carbon relaxation samples. See Materials and Methods for details.

binary state indicate that the polypeptide chain is predominantly rigid, ranging from 0.67 to 1.0 with an average value of 0.927. These data are compiled in Table S4 and are deposited to the BMRB under accession number 18251.

The ternary (Cdc42Hs·GMPPCP–PBD46) complex state had 122 resolved N–H probes. Fifty-four probes were excluded from the τ_m calculation for the reasons described above. The remaining 68 probes were subsequently analyzed to determine the tumbling characteristics of the Cdc42Hs·GMPPCP–PBD46 complex. The macromolecular tumbling was best fit to an isotropic model with a tumbling time of 16.7 ± 0.1 ns (Table 1). With the use of this rotational correlation time, model-free and R_{ex} parameters were fit for all 122 probes. Twenty-one of these sites then showed statistically significant R_{ex}. O^2_{NH} values ranged from 0.737 to 1.0 with an average of 0.945, indicating that the protein backbone remains generally rigid after binding to PBD46. These data are compiled in Table S5 and are deposited to the BMRB under accession number 18252.

As has been observed with many other proteins [39], backbone amides in both states of the protein examined are largely rigid and pairwise differences are generally small. The difference in average O^2_{NH} upon binding PBD46 ($\Delta\overline{O^2_{NH}}$) and the average of the differences in O^2_{NH} across the 105 probes available in both the ternary and binary complexes ($\overline{\Delta O^2_{NH}}$) yielded nominally positive values of 0.018 (±0.009) and 0.015 (±0.009), respectively, on binding the PBD46 to Cdc42Hs·GMPPCP (Table 2). No structural or sequence-based correlations are apparent.

Table 2. Effects of binding of PBD46 to the binary Cdc42Hs·GMPPCP complex on the motion of amide backbone bond vectors and methyl-bearing side chains in Cdc42Hs determined by amide nitrogen and methyl carbon relaxation, respectively

	$\Delta\overline{O^2}$[a]	$\overline{\Delta O^2}$[b]
ΔO^2_{NH}	0.018 (±0.009)	0.015 (±0.009)
ΔO^2_{axis}	0.053 (±0.027)	0.060 (±0.028)

[a] $\Delta\overline{O^2}$ is the change in average order parameter (ternary complex–binary complex) and does not require pairwise comparisons; all measureable probes were used.
[b] $\overline{\Delta O^2}$ is the average change in order parameter and requires pairwise comparisons.

Methyl-bearing side-chain dynamics

With the use of a pyruvate-based isotopic labeling strategy [33,40], Cdc42Hs was labeled to produce methyl groups with $^{13}C^1H^2D_2$ as the principle isotopomer and low amounts of extraneous nonbonded ^1H spins. Of the 120 possible methyl probes, four relaxation rates were satisfactorily obtained for 91 and 86 sites in the binary (Cdc42Hs·GMPPCP) and ternary (Cdc42Hs·GMPPCP–PBD46) complexes, respectively. This produced 79 specific pairwise probes. T_1 and $T_{1\rho}$ values are compiled in Table S6.

Carbon methyl axis squared generalized order parameters (O^2_{axis}) were calculated for the $^{13}C^1H^2D_2$ isotopomer from four determined rates (T_1 and $T_{1\rho}$ at 14.1 and 17.6 T) for each state. Contributions to dipolar relaxation from both deuterium and proton spins were included [Eq. (3)] in the determination of Lipari–Szabo model-free parameters. In addition, contributions from chemical shift anisotropy (CSA) relaxation [33] and from dipole–dipole relaxation of remote nuclei calculated on a per-probe basis by the effective distance to each remote nucleus [34] were also included [see Eq. (3)]. Assuming no cross-correlation effects (which are suppressed by ^1H decoupling during relaxation), on average, ~90% of the R_1 rate comes from the relaxation of the C–H methyl dipole–dipole interaction, ~10% comes from the two C–D dipole–dipole interactions, 0.6% comes from the CSA and less than 0.5% comes from all external dipolar nuclei. Similarly, the $R_{1\rho}$ rate is composed of 80% C–H methyl dipole–dipole, 7.5% from the two C–D dipole–dipole interactions, 12% from the CSA and less than 0.5% from all external dipolar nuclei. The methyl O^2_{axis} values in the binary state averaged to 0.671 with a range from 0.135 to 1.0, while the average value over all of the ternary probes was 0.724 with a range from 0.081 to 1.0. Methyl O^2_{axis} and τ_e values are compiled in Table S7 and are deposited to the BMRB under accession numbers 18251 and 18252.

Nanosecond-to-picosecond dynamics of Cdc42Hs·GMPPCP and Cdc42Hs·GMPPCP–PBD46 methyl groups have been studied previously using deuterium relaxation methods [32]. The isotropic tumbling model determined here for the ternary state is consistent with that study. However, the molecular tumbling model for the binary complex determined here is axially symmetric, not the isotropic tumbling model used in the previous study. Both the present analysis and the previous study conclude that there are relatively small changes in the backbone amide bond vector motions [31]. Importantly, the results reported here for the side-chain motions differ in several significant respects. Though there are slight differences in solution conditions, we largely attribute the differences in characterization of side-chain motion to the NMR relaxation methodology employed. The prior study was undertaken with the original deuterium relaxation experiments of Muhandiram *et al.* [41], which are sensitive to fast deuterium relaxation mechanisms during the $^{13}C–^{2}H$ coherence transfer steps [34,41,42]. Consequently, as macromolecular tumbling slows, a general degradation in signal-to-noise ratio will occur, particularly for those sites with short ^{2}H transverse relaxation times (corresponding to rigid sites with high order parameters). The ternary Cdc42Hs·GMPPCP–PBD46 complex tumbles with a 17-ns macromolecular correlation time (Table 1), in a regime where the efficiency of the INEPT-based $^{13}C–^{2}H$ coherence transfers of the deuterium relaxation experiments, designed for small, rapidly tumbling proteins, competes with ^{2}H longitudinal relaxation ($T_1 < 25$ ms). The effects of the relaxation are 2-fold: reduction in the reliability of obtained order parameters with increasing magnitude of O^2_{axis} and the loss of a substantial number of the more rigid sites for which no information is available thus introducing a bias toward mobile sites with more favorable relaxation properties. In contrast, the carbon relaxation experiments utilized here are essentially insensitive to the macromolecular tumbling regime of the binary and ternary complexes of Cdc42Hs [34,43]. The reliability effect can be seen in the magnitude of estimated errors of the previously determined O^2_{axis} parameters and the order parameters determined in this study (Fig. S1). The precision of the O^2_{axis} parameters based on methyl carbon relaxation is approximately a factor of 2, better than for those determined previously using O^2_{axis} parameters based on methyl deuterium. In addition, the bias against rigid (high O^2_{axis}) sites will confound a subsequent interpretation of the "dynamical proxy" for conformational entropy due to the sensitivity of such interpretations to both the degree of methyl probe coverage of the protein and their quantitative reliability [23,25]. Here 79 pairwise comparisons were measured, while the previous study measured only 40 (Table S3). This results in significantly higher precision and provides a more complete and somewhat different view of the dynamical response of Cdc42Hs to the binding of PBD46, as described below.

Three classes of fast motion of methyl-bearing side chains, termed J, α and ω, are often revealed by NMR relaxation [23,44]. The J-class is usually centered around an O^2_{axis} value of ~0.35 and involves motion of the methyl group between rotameric wells, leading to averaging of the associated J-coupling. The α-class is usually centered around an O^2_{axis} value of ~0.65 and has smaller contributions from motions that lead to rotameric interconversion and largely reflects large amplitude motion within a single rotameric well. The ω-class is centered around an O^2_{axis} value of ~0.85 and has highly restricted motion within a single rotameric well that is equivalent to the uniform rigidity of most backbone sites. As has been seen previously with other proteins [23], the distributions of O^2_{axis} parameters of the binary and ternary complexes reflect a tri-modal distribution of motional states (Fig. S2). Both the binary and the ternary states of Cdc42Hs exhibit relatively low populations of the α-class and enriched contributions from the ω-class. These distributions suggest that both states of the protein are relatively rigid, with the ternary complex being unusually enriched in the ω-class. These results contrast sharply to that seen previously [32].

Changes in internal motion of Cdc42Hs upon binding of PBD46

Methyl-bearing side chains in the binary complex have O^2_{axis} values ranging from 0.135 to 1.0 while those in the ternary complex range from 0.08 to 1.0. Significant differences in O^2_{axis} values between the binary and ternary complexes are seen across the Cdc42Hs protein (Fig. 2 and Table S7). Not all Cdc42Hs methyl sites become more rigid upon binding PBD46. The distribution of ΔO^2_{axis} values fits well to a single Gaussian function ($R = 0.98$). A simple "thermodynamic particle" view of the evolutionary pressure utilizing contributions of conformational entropy (see below) to adjust the total entropy of binding would naturally give rise to such a distribution [23], yet a number of probes apparently fall outside this simple distribution, suggesting that something more interesting is going on. An iterative analysis using the interquartile range method [45] was employed to objectively identify outlier sites. Nine methyl probes in Cdc42Hs having distinguishingly large changes in motion upon binding of PBD46 were highlighted by this analysis: Val7γ2, Thr17γ2, Ile21γ2, Val42γ2, Val44γ2, Ile46δ1, Leu111δ1, Leu129δ1 and Leu129δ2. They are predominantly located near the binding interface with PBD46 and suggest the initiation of a dynamic signaling mechanism. Upon binding to Cdc42Hs, PBD46 provides an additional strand to an existing β-sheet that lies across most of the binding interface (Fig. 1). The probes experiencing the greatest spatial restriction, Val42γ2 and Ile46δ1, are located on the

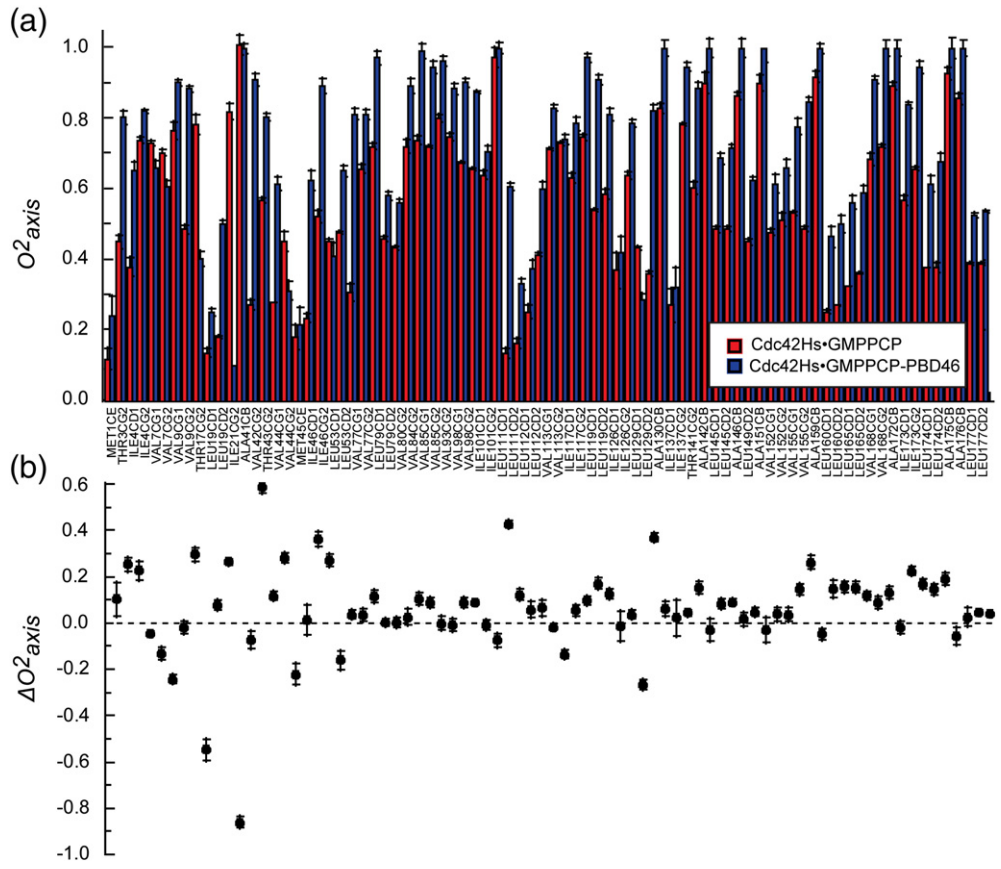

Fig. 2. Motional character of methyl-bearing side chains in the binary (Cdc42Hs•GMPPCP) and ternary (Cdc42Hs•GMPPCP•PBD46) complexes of Cdc42Hs. (a) Bar graphs of the O^2_{axis} values for the methyl groups of Cdc42Hs in the binary (red) and ternary (blue) complexes. (b) Site-to-site differences (ΔO^2_{axis}) of the ternary complex minus the binary complex.

β-sheet with direct contact to PBD46. The Leu129δ1 and Leu129δ2 probes form a set of Gaussian outliers that demonstrate opposite dynamic responses, more rigid and more flexible, on binding PBD46. They are located in the Rho insert helix remote from the PBD46 binding interface. Side chains of methyl-bearing probes provide about one-quarter of the intermolecular binding surface and are seen to respond heterogeneously with nominally no net change in order parameter at the intermolecular interface. This perhaps counterintuitive response is also observed in the calmodulin–peptide complexes [25]. This can be likened to a "rippled effect" for the dissipation of the motional perturbation in response to a binding event. A simple physical model describing the interactions between closely packed side chains predicts this type of behavior [44].

Structural correlations of changes in methyl dynamics

There is a heterogeneous distribution of motional changes (ΔO^2_{axis}) in Cdc42Hs on moving from the binary Cdc42Hs•GMPPCP complex to the Cdc42Hs•GMPPCP–PBD46 ternary complex (Fig. 3a). Color coding of methyl groups by the magnitude of the change in their motion (ΔO^2_{axis}) visually exposes several trends (Fig. 3b). Methyl probes in Cdc42Hs experiencing the largest change in motion upon binding PBD46 are generally located at or close to the binding interface. It is important to emphasize that the degrees of increased flexibility and rigidity are not equal and that not all sites near the interface of Cdc42Hs with PBD46 show large changes in flexibility. Indeed, many methyl probes show no perturbation in their motion upon binding. A striking exponential relationship is observed between the *statistical variance* of ΔO^2_{axis}, which reflects the absolute magnitude of dynamical perturbation, and the nearest distance of the methyl probe to the bound PBD46 (Fig. 4a). Here we use the standard statistical definition of variance to describe the magnitude and heterogeneity of the dynamical response to binding of PBD46. Probes that fall closest to the PBD46 domain have the greatest variance among their ΔO^2_{axis} values while

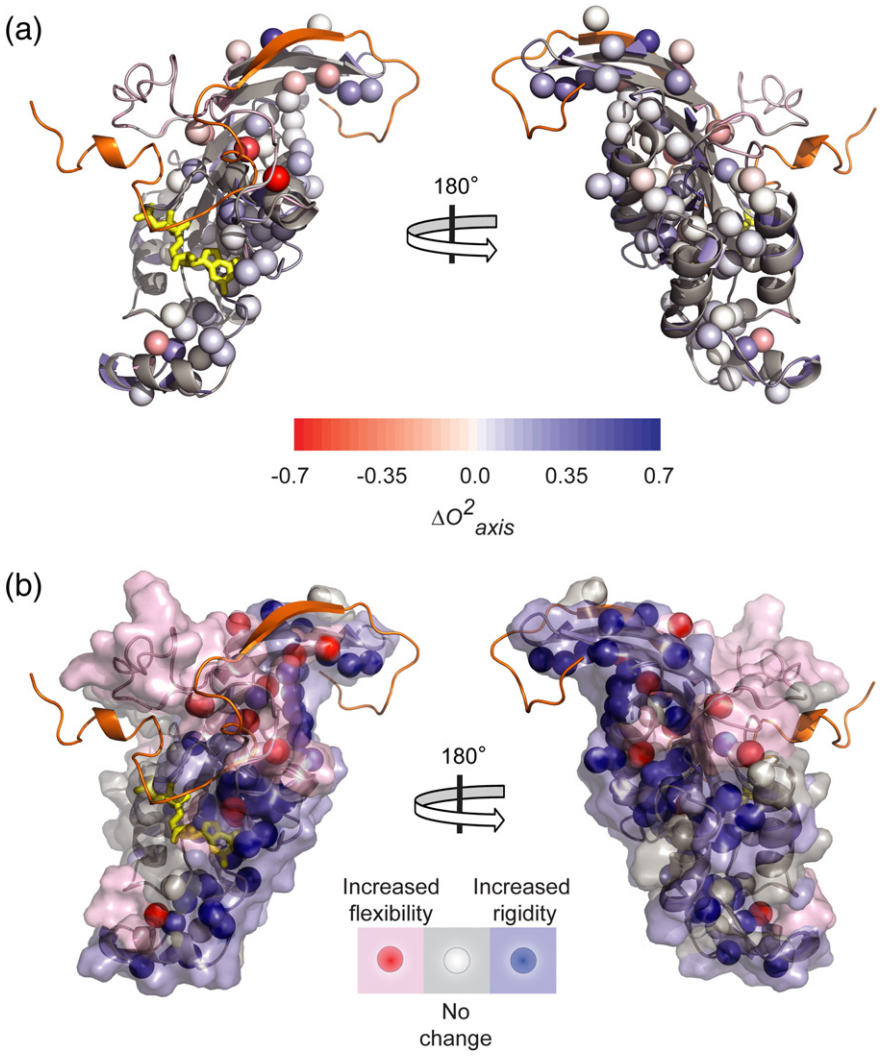

Fig. 3. Two views of methyl order parameter changes upon binding PBD46 to Cdc42Hs·GMPPCP (PDB ID: 1EES [14]). In both views, the backbone ribbon representation of Cdc42Hs is shown in gray with PBD46 in orange. Methyl probes with relaxation data in both ternary and binary states are shown as spheres. In (a), the methyl probes are colored according to the degree of change ΔO^2_{axis} (see inset color scale). The darkest spheres indicate probes with the largest magnitude of ΔO^2_{axis}. In (b), ΔO^2_{axis} values upon binding PBD46 are grouped into three categories to highlight the spatially localized dynamic response of Cdc42Hs to the binding of PBD46. Red spheres represent probes that become more flexible ($\Delta O^2_{axis} < 0$), blue spheres represent probes that become more rigid ($\Delta O^2_{axis} > 0$) and white spheres represent probes whose change is within error of zero. The surface rendering of Cdc42Hs is colored according to the closest measured probe.

the probes farthest from the binding site have ΔO^2_{axis} values within error of zero. Indeed, the variance of the dynamical response to binding falls off exponentially with a decay constant of 0.568 ± 0.090 $Å^{-1}$ (Fig. 4b), suggesting that motional coupling is limited. Studies using double-mutant cycles on small proteins have suggested that, in single-domain proteins, residues close in space have a higher likelihood of thermodynamic coupling than those further away [46–48]. The results presented here are consistent with this view. A similar observation has been observed in molecular dynamics trajectories where a correlation of dihedral angles is apparent [49].

There is a set of outliers to the observed *variance* of the dynamic response of Cdc42Hs on binding PBD46 (Fig. 4a). These residues fall into two structural groups. V42γ2 and I46δ1 participate in an intermolecular β-sheet formed on binding PBD46 and become more rigid. V7γ2, I21γ2 and T17γ2 reside in secondary structure elements that line the GTP-binding pocket and show increased flexibility upon formation of the complex. L129δ1 and L129δ2 are located in the distal Rho insert region that demonstrate a disparity in the dynamic response, both rigidification and increased flexibility of the methyl groups on the same leucine.

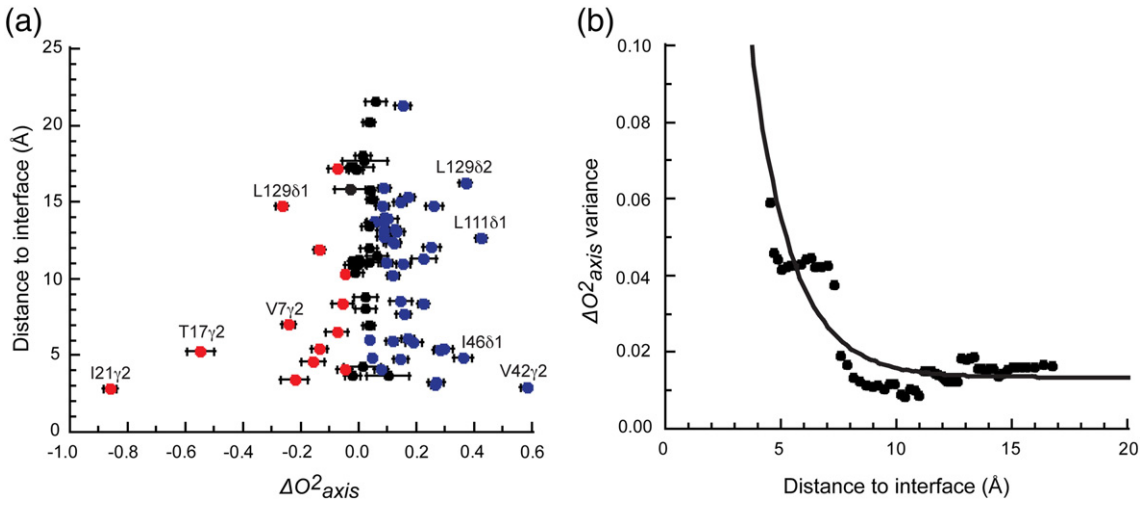

Fig. 4. Propagation of dynamical perturbation of Cdc42Hs upon binding of PBD46. (a) Spatial profile of methyl order parameter changes *versus* distance to the PBD46 molecule. Errors bars are based on Monte Carlo estimates of the precision of the individual O^2_{axis} values. Probes with ΔO^2_{axis} within their error of zero are colored as black circles, those with increased flexibility upon binding are colored red and those with increased rigidification upon binding are colored blue. Extremes of the dynamic perturbation are identified by their residue name. (b) Probes were ordered based on their distance to the PBD46 molecule and a 20-element moving window approach was used to calculate the rolling mean and variance. The variance of ΔO^2_{axis} for each window is plotted against the average distance to the nearest PBD46 atom within the window. The continuous line results from an exponential decay fit ($y = a + be^{-cx}$) with an R value of 0.89 (where $a = 0.0138 \pm 0.0014$, $b = 0.72 \pm 0.31$ and $c = 0.568 \pm 0.090$ Å^{-1}).

Thermodynamic consequences of modulation of motion in Cdc42Hs upon binding PBD46

The binding of PBD46 results in a net reduction in the motion of methyl-bearing side chains in Cdc42Hs (Table 2 and Fig. 2). The difference in the average O^2_{axis} of each complex (ΔO^2_{axis}) was found to be 0.053 ± 0.027. Averaging over the 79 probes with data in both states gave a similar value (ΔO^2_{axis}) of 0.060 ± 0.028. The modest net decrease in methyl-bearing side-chain motion in Cdc42Hs upon the binding of PBD46 suggests a correspondingly small unfavorable decrease in conformational entropy, since changes in internal motion reflect changes in conformational entropy. Marlow *et al.* established a quantitative linear relationship between average changes in side-chain motion and corresponding changes in conformational entropy [25]. This empirical calibration of the change in NMR-derived generalized order parameters with protein conformational entropy has recently been refined [26]. The key step is the projection of changes in the dynamics of the methyl probes across the entire protein molecule. Initially performed simply using the number of residues [25], it is now clear that the number of side-chain χ torsion angles provides a more appropriate scaling. The difference of the averages of methyl-bearing side-chain dynamics in the Cdc42Hs molecule upon binding PBD46 (i.e., ΔO^2_{axis}) is therefore multiplied by the 330, which corresponds to the total number of side-chain χ torsion angles present in Cdc42Hs. The experimentally determined conversion factor of -0.0019 ± 0.0001 kcal mol^{-1} K^{-1} torsion^{-1} is used to recover the change in conformational entropy [26]. The PBD46 ΔO^2_{axis} was not measured in this analysis. Therefore, the contribution by PBD46 represents an uncertainty. Two extremes in dynamical response of PBD46 to formation of the complex can be envisaged. One would be that the disordered free PBD46 domain remains as dynamic upon binding corresponding to no change in ΔO^2_{axis}. The other extreme would correspond to PBD46 becoming fully rigid upon binding. There are 24 side-chain χ torsion angles present in PBD46. These two scenarios result in the error bars shown in Fig. 5.

The scaling of the dynamical proxy of Cdc42Hs binding PBD46 in terms of a change in conformational entropy is fully consistent with that established by the calmodulin [25] and catabolite activation protein [50] systems (Fig. 5). The total binding entropy (ΔS^{tot}) was obtained from ITC [51]. The ΔS_{solv} for the binding of Cdc42Hs to PBD46 is evaluated [52] from the change in polar and nonpolar solvent-accessible surface area (ASA) [53]. The ASA of the ternary complex was calculated using the 1EES PDB structure file [14] with the GMPPCP molecule positioned as in the binary complex (2QRZ) [54] of the 178-residue Cdc42Hs bound to the 46-residue PBD46. The ASA of the binary complex was evaluated from the 2QRZ PDB structure file [54] with the 189 residues of Cdc42Hs truncated from the carboxyl terminus to the comparable 178 residues in 1EES [14]. The GMPPCP molecule was

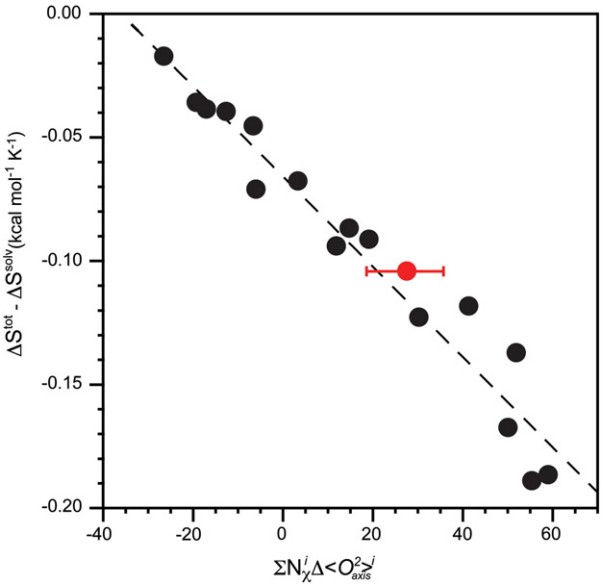

Fig. 5. Consistency of the apparent change in conformational entropy of dynamical response Cdc42Hs binding of PBD46 to the "conformational entropy" meter calibration established by calmodulin and the catabolite activation protein. Black-filled circles correspond to both wild type and mutant catabolite activator protein binding to DNA and calmodulin binding to various peptides representing calmodulin-binding domains of regulated proteins [26]. For Cdc42Hs·GMPPCP binding PBD46, the total binding entropy (ΔS^{tot}) was obtained from ITC [32]. The calculated ΔS_{solv} for Cdc42Hs binding PBD46 is entropically favorable at +0.104 kcal mol^{-1} K^{-1}. Cdc42Hs·GMPPCP binding PBD46 (red-filled circle) results in excellent agreement with the calibration line established by catabolite activator protein and calmodulin. The error bar associated with Cdc42Hs·GMPPCP binding PBD46 results from very conservative assumptions regarding the range of change in motion of PBD46 upon binding (see the text). The empirical scaling of observed changes in motion with entropy (slope) is −0.0019 ± 0.0001 (kcal mol^{-1} K^{-1}).

included in the ASA of the binary complex. The ASA of the free 46-residue PBD46 molecule was extracted from the PDB structure file 1EES [14] and treated as the free peptide maintaining the 6-residue helix with the remainder of the peptide essentially random coil. The ΔS_{solv} for the binding of PBD46 to Cdc42Hs is an energetically favorable +0.104 kcal mol^{-1} K^{-1}. The NMR-derived change in conformational entropy ($-T\Delta S_{conf}$) for the Cdc42Hs upon binding PBD46 is determined to be +9.8 kcal mol^{-1} at the temperature used here (298 K). This compares to the total binding entropy ($T\Delta S^{tot}$) obtained from ITC of −2.4 kcal mol^{-1} at 298 K. The previously reported NMR-derived change in conformational entropy ($T\Delta S_{conf} \sim -5$ kcal mol^{-1} [32]) is of opposite sign to the present study. The thermodynamic parameters of the binding of Cdc42Hs·GMPPCP to PBD46 are summarized in Table 3.

Illumination of a potential allosteric network in Cdc42Hs

The rapid dissipation with the distance of the perturbation of motion in Cdc42Hs upon binding the PBD46 (Fig. 4) indicates the presence of limited dynamical coupling through the protein. We observe that a subset of sites becomes more rigid ($\Delta O^2_{axis} > 0$) and a subset becomes more flexible ($\Delta O^2_{axis} < 0$) upon binding PBD46. These subsets distribute into two spatially separate clusters that bisect the molecule through the nucleotide-binding site (Fig. 3b). There is an increased rigidity distributed along the long axis of the Cdc42Hs opposite the predominant binding surface of the PBD46. The cluster of the long axis that contains the PBD46 binding interface shows an overall increased flexibility. K-means spatial clustering confirms their statistical significance ($p < 0.02$). The inherent slow timescale (microseconds to milliseconds) dynamics of residues in the Switch I and Switch II regions of Cdc42Hs [14,35,55] compromise the determination of changes in methyl-bearing side-chain motion on the faster picosecond-to-nanosecond timescale. The closest probes to Switches I and II are unaffected by the binding of PBD46. Nevertheless, Switch I is located in the region of Cdc42Hs that becomes more rigid upon binding of PBD46, while Switch II is located in the region that becomes more flexible. The asymmetry of the dynamic response suggests that the binding of PBD46 to the activated Cdc42Hs can modulate the directional bias of the response and that a dynamical allosteric network may be present in Cdc42Hs.

This apparent bifurcation of the dynamic response separated along the long axis of the Cdc42Hs is orthogonal to the nucleotide-binding pocket (Fig. 6a). The methyl sites are colored in three groupings according to the ΔO^2_{axis}: red spheres indicate increased flexibility, blue indicates increased rigidity

Table 3. Thermodynamic properties of the binding of PBD46 to the binary Cdc42Hs·GMPPCP complex

	K_D (nM) [35]	ΔH (kcal mol^{-1}) [51]	ΔS^{tot} (cal mol^{-1} K^{-1})	ΔS_{solv} [a] (cal mol^{-1} K^{-1})	$-T\Delta S_{conf}$ (kcal mol^{-1})
ITC	20	−13	−8.4	−104	
NMR (present study)					+9.8
NMR (Loh *et al.* [32])					−5.0

[a] The change in solvent entropy was evaluated according to the fractional contributions of polar and apolar ASA as described by D'Aquino *et al.* [53].

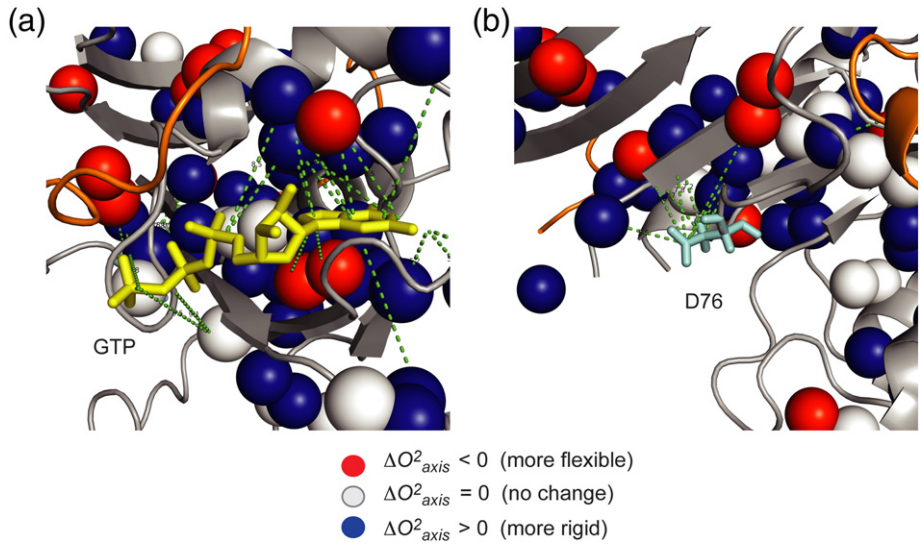

Fig. 6. Detailed view of the dynamical perturbation of the GTPase enzyme active site. (a) The nucleotide-binding pocket in relation to the dynamic network is illuminated here for Cdc42Hs binding to PBD46. Cdc42Hs and PBD46 are colored as in Fig. 3b. Modeled in yellow is the GTP molecule, aligned within the frame of Cdc42Hs using a homologous structure (PDB ID: 2QRZ [54]). Methyl groups with pairwise measured ΔO^2_{axis} values upon binding PBD46 are represented by spheres grouped into three categories indicated by the color key. Distances less than 10 Å are indicated between the measured methyl probes and the guanine ring atoms or the triphosphate atoms. (b) The highly conserved aspartate 76 residues of Cdc42Hs (colored cyan) are involved in the GTPase action of Cdc42Hs [56]. Distances less than 10 Å are indicated between the measured methyl probes and the C^{γ} and C^{β} atoms of D76.

and gray represents no dynamical change on binding PBD46. The GTP-binding pocket shows both rigidification and increased flexibility. Green broken lines indicate guanosine atoms that are within 10 Å of a measured methyl probe. There is an overall increased rigidity observed surrounding the α and β phosphate positions of the triphosphate moiety while the γ phosphate sees no change in the motion of surrounding methyls. Increased motion is observed above and below the plane of the purine ring. In contrast, in the plane of the purine ring, there is increased rigidity in methyl-bearing side chains. The dynamic response within 10 Å of a methyl probe at the D76 C^{γ} and C^{β} side-chain atoms shows an overall rigidification at the catalytic carboxyl group of D76 (Fig. 6b). Thus, the dynamical response at the GTP-binding site and the conserved D76 catalytic residue [56] is complex. The rate of GTP hydrolysis [35] with PAK bound is slowed relative to the PAK free activated state of Cdc42Hs. The downstream effector binding to GAP in response to PAK binding to Cdc42Hs promotes the enzymatic hydrolysis of the γ phosphate. The rigidification of atoms involved in the catalytic event with PAK binding could potentially trap the GTP moiety preventing the sampling of the transition state for hydrolysis and thereby slowing the reaction rate. The binding to the GEF, a regulator of the activated GTPase, in response to the PAK binding to Cdc42Hs enhances the molecular diffusion swapping GDP for GTP. The increased flexibility axial to the guanine ring could potentially assist the diffusion of the GDP molecule out of the binding pocket as it exchanges for an incoming GTP molecule.

The catalytic activity of the Ras protein family has been the subject of much experimental and theoretical attention [57,58]. The lack of experimental evidence of a transition state structure is at the heart of a controversy. While this study does not provide a structural presentation of the transition state, it does provide an experimental dynamical snapshot of the accommodation required for its formation. The rigidification identified in the GTP pocket in response to binding the PAK CRIB domain to Cdc42Hs is consistent with the slowed rate of GTP hydrolysis imposed by the binding event [32].

The network of dynamical coupling (Fig. 7a) does not have a corresponding structural component on binding PBD46. Changes in amide ^{15}N and ^{1}H chemical shifts are often used as an indicator of a structural response to a ligand binding event [59]. Figure 7 depicts the dynamical response juxtaposed with the structural response. The region of significant chemical shift changes maps to the contact surface of the PBD46 that contains the Switch I and II regions of Cdc42Hs [35]. Smaller chemical shift changes are observed in the GTP-binding pocket. There are no significant changes in chemical shifts at sites remote from the binding surface in particular for the Rho insert region. The chemical shift changes of the Cdc42Hs backbone amide resonances on binding PBD46 ($\Delta\delta^{15}N–\delta^{1}H$) are plotted (orange) as a function of Cdc42Hs residue number along with the dynamical

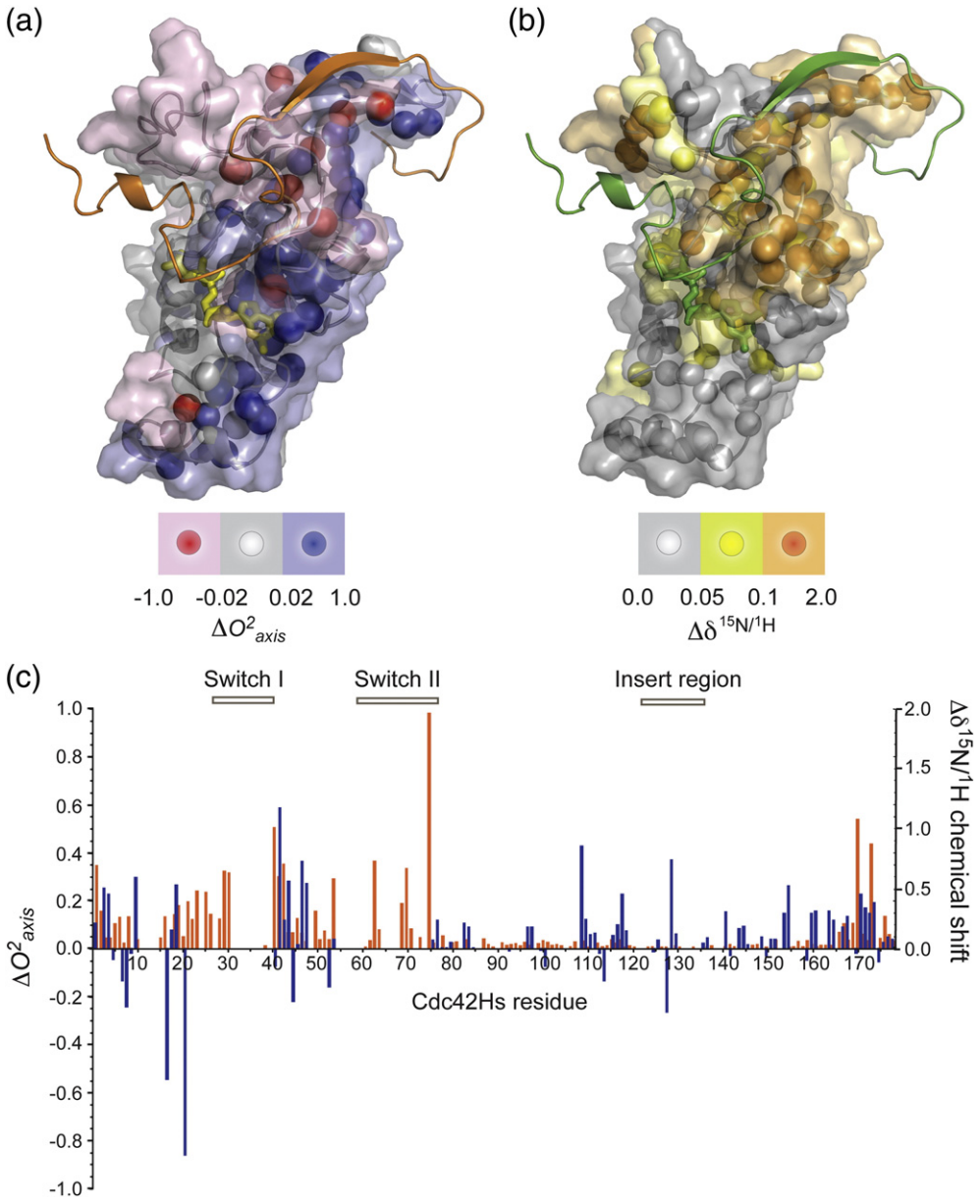

Fig. 7. Comparison of the structural and dynamic perturbations on binding the PAK-binding domain PBD46 to Cdc42Hs. (a) Mapping the ΔO^2_{axis} onto the structure of Cdc42Hs·GMPPCP·PBD46 (PDB ID: 1EES) [14]. Cdc42Hs and PBD46 are colored as in Fig. 3b. The change in the methyl axis order parameters is colored according to the key. (b) The amide chemical shift differences $[(\Delta\delta^{15}N\ \gamma_{15N}/\gamma_{1H})^2 + (\Delta\delta^1H)^2]^{1/2}$ are mapped onto the structure of the Cdc42Hs·GMPPCP·PBD46 (PDB ID: 1EES) [14]. Chemical shift differences are a virtual reporter of structural changes on complexation [59]. The PBD46 peptide and the GMPPCP molecule are shown in green. The GMPPCP molecule is modeled into the complex using (PDB ID: 2QRZ) [54]. The color code is shown in the inset bar, with orange showing the most significant chemical shift differences, yellow showing subtle changes and gray showing virtually no change on binding the PBD46 peptide. (c) The dynamic response (ΔO^2_{axis}) and the structural response ($\Delta\delta^{15}N/^1H$ chemical shift) are plotted according to the Cdc42Hs residue number. The ΔO^2_{axis} data are colored blue, and the $\Delta\delta^{15}N/^1H$ chemical shift data are colored orange. There is a significant dynamical response yet no structural response that localizes to the Rho insert region of the complex.

change in ΔO^2_{axis} (blue) (Fig. 7c). There is a distinct absence of chemical shift change at the Rho insert helix. This is the region that demonstrates significant dynamical outliers in the *variance* of the ΔO^2_{axis} to the distance from the ligand (Fig. 4a). This is a strong indication of a long-range dynamical but not structurally mediated response to the binding event. This observation strongly supports the need to view allostery in

the context of the ensemble of states [60], particularly those that carry with them significant entropy. It is clear here that the perturbations of fast motions connecting states closely similar to the average structure contribute significantly to the free energy of binding.

This analysis of the dynamic network provides the visualization of the apparent propagation from the PBD46 binding surface to the Rho insert helix. The distal Rho insert helix of Cdc42Hs seems to be the action point for the dynamically mediated signal transduction to downstream effector molecules. The Rho insert region has previously been described as a "foot-rest" for docking of regulatory and effector proteins [5] and identified as a hallmark of Rho proteins involved in effector binding and specificity [61]. Our analysis suggests that when the activated Rho GTPase is suppressed by PAK binding, the Rho insert region responds dynamically but not structurally (i.e., the mean structure remains the same) in the facilitation of downstream effector protein binding.

Implications for other interactions in the Cdc42 signaling network

Over the past several decades, the classical view of biochemical signaling pathways as a linear series of discrete switching events has been replaced by the notion of integrated signaling networks. Many proteins bind to more than a single partner and forward, reverse and cross-signaling have all been documented [62]. Despite its classification as a molecular switch, the interaction of Cdc42Hs with downstream components of the signaling pathway is complicated by the presence of a variety of feedback loops and opportunities for cross-talk. While many of the interactions of the Rho GTPase with multiple downstream effector proteins seem to be modulated via scaffolding proteins [63–65], there are reports of Cdc42 participating in the integration of signal transduction pathways. For example, knockout studies in yeast show a two-pronged signaling path to the activation of the actin-related protein complex 2/3 downstream of Cdc42Hs involving PAKs and certain other effector proteins, specifically formin homologs [66]. Thus, downstream actin polymerization responses are mediated through both PAK-like component and formin-like component. It has been suggested that they are linked via Cdc42 through formation of a ternary intermediate complex [66,67]. In addition to downstream effectors, Cdc42 and other similar GTPases interact with a variety of activity-modulating proteins, mainly GEFs, GAPs and GDIs. Simultaneous interaction of Cdc42 with both GAPs and CRIB-containing proteins has not been shown to date, but GEFs have been found to form ternary intermediates with Cdc42 and PAK [68,69].

The potential for a range of ternary interactions involving the Cdc42·PBD46 raises the possibility that dynamical perturbations remote from the Cdc42·PBD46 interface may be important in the signaling cascade. Structural alignment of multiple Cdc42–protein complexes is illustrative. Though Cdc42 adopts a slightly different conformation in each complex, formins, GEFs, GDIs and GAPs can all bind to the same face of Cdc42, but GAPs such as Cdc42GAP form a larger interface. Steric exclusion does not appear to prevent the formation of a Cdc42·GAP·PAK complex; the only steric clashes between PBD46 and GAP in the aligned structures are at the disordered region of PBD46 from the NMR-based structural model [14]. The additional segment of the interface not present with the GEF and formin complexes, however, corresponds to the section of Cdc42Hs that is dynamically activated by the binding of PBD46. Several of these interaction complexes are illustrated in Fig. 8 superimposed with the dynamical response to PAK binding color coded onto the Cdc42Hs molecule. The top two complexes typify downstream effector proteins binding to the activated GTPase, a GAP and a formin. The bottom two complexes are of two regulatory proteins, a GDI and a GEF that bind the GTPase in response to the conversion of GTP to GDP, converting Cdc42Hs to the inactive state. The alignment of the structures of Cdc42·PBD46 (PDB ID: 1EES) [14] with Cdc42·RhoGDI (PDB ID: 1DOA) [73] indicates that Cdc42Hs complexed with the PBD46 PAK CRIB domain would not accommodate RhoGDI as a ternary complex without reorganization to avoid significant steric clashes.

The binding of a GAP in response to the PAK CRIB domain binding to Cdc42Hs has not been captured as a ternary complex. Figure 8a shows the alignment of Cdc42·PBD46 (PDB ID: 1EES) [14] color coded according to the dynamical response of the activated Cdc42Hs binding to PBD46 with Cdc42GAP (PDB ID: 1GRN) [56] colored yellow. The binding interface of the Cdc42Hs with the Cdc42GAP has an overlap in the Switch I and Switch II domains and a significant surface area of interaction at the Rho insert region of Cdc42Hs. The Cdc42GAP has its binding interface parallel with the long axis of the Cdc42Hs molecule. The bifurcated dynamic response that is observed on binding PBD46 is positioned such that the more flexible surface is juxtaposed at the interface of the Cdc42GAP with Cdc42Hs·GMPPCP·PBD46. The Rho insert region displays a dynamical response yet shows no significant structural change as monitored by chemical shift differences (Fig. 7a and b) and apparently propagates an allosteric dynamic response to the surface where significant interaction with Cdc42GAP occurs. Both Switches I and II interact with the GAP protein. Switch II plays an important direct mechanistic role in the hydrolysis of GTP that is promoted by GAP binding to a dynamically flexible region of Cdc42Hs. The GAP conserved residue R305 is positioned for catalysis [70,71] in a rigidified pocket of

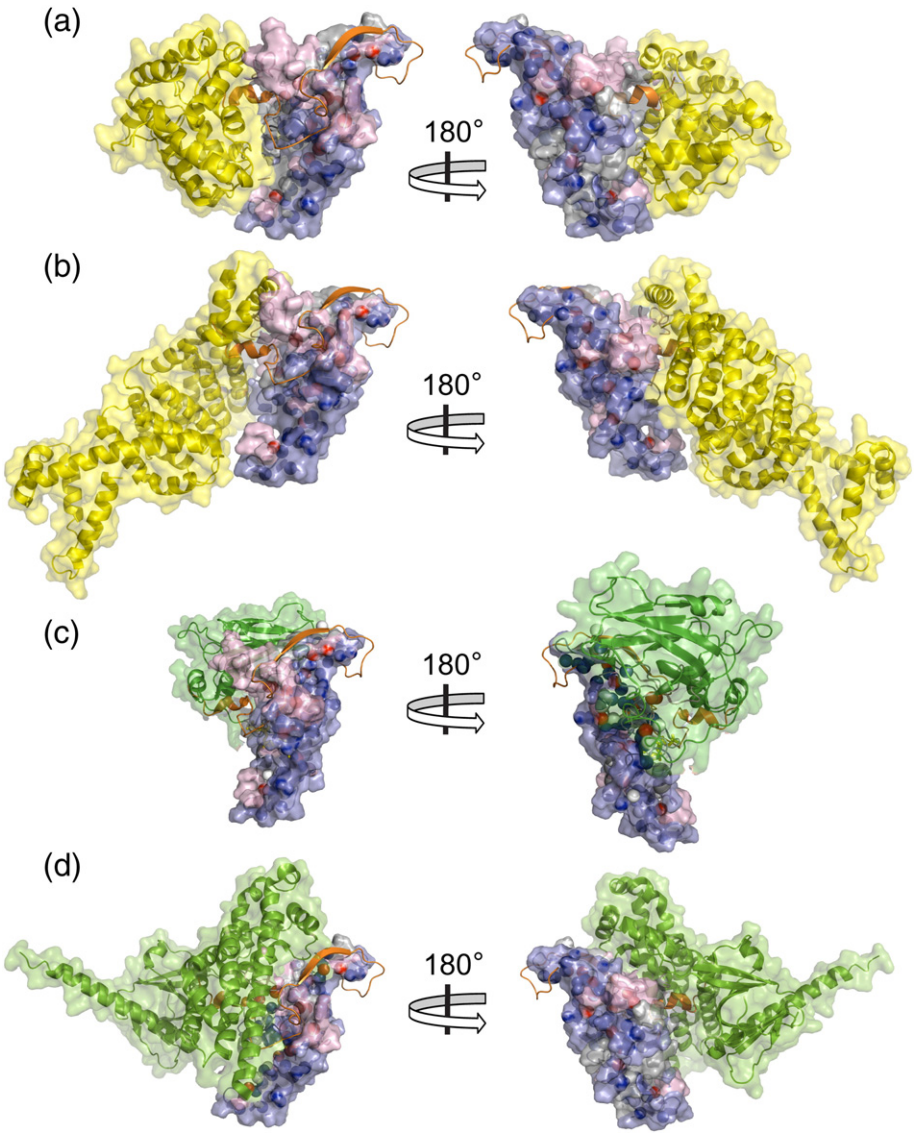

Fig. 8. Models of the aligned Cdc42Hs·GMPPCP·PBD46 with effector/regulator complexes. Cdc42Hs·GMPPCP·PBD46 is rendered using the scheme of Fig. 3b where the color coding indicates the dynamical response in O^2_{axis} on binding the PAK domain (PBD46) to the GTP-bound activated state of Cdc42Hs, blue is more rigid, red is more flexible and gray is no change. The alignments are fit using the common Cdc42Hs molecule of both structures as the target with the PyMOL align function [89]. (a) The alignment of Cdc42Hs·GMPPCP·PBD46 (PDB ID: 1EES) [14] with Cdc42·Cdc42GAP (PDB ID: 1GRN) [56] in yellow. The GAP is positioned in such a way that the PBD46 when bound to Cdc42Hs would accommodate the ternary complex. (b) The alignment of Cdc42Hs·GMPPCP·PBD46 (PDB ID: 1EES) [14] with the effector protein formin, mDia (PDB ID: 3EG5) [61] in yellow. The major binding interface contains the PBD46 binding interface, the Switch II region and the Rho insert helix. (c) Cdc42Hs is complexed with the regulatory protein GDI (Rho GDI). The alignment of the structures of Cdc42Hs·GMPPCP·PBD46 (PDB ID: 1EES) [14] with Cdc42·RhoGDI (PDB ID: 1DOA) [73] shown in green. The alignment encapsulates the PBD46 binding interface, the GTP-binding pocket and the Switch I and II domains but lacks interaction with the Rho insert region. (d) Cdc42Hs has been documented to accommodate simultaneous interactions with PAKs and guanosine exchange factors (GEFs) [68,69]. The alignment of the structures of Cdc42Hs·GMPPCP·PBD46 (PDB ID: 1EES) [14] with Cdc42·Dbs GEF (PDB ID: 1KZG) [74] is shown in green. A similar binding interface is observed for both regulatory proteins, lacking any apparent contact with the Rho insert region.

Cdc42Hs, which is consistent with the pre-organization view of catalysis [72]. For all of the Cdc42Hs complexes evaluated in Fig. 8, both effector and regulatory proteins, the surface of Cdc42Hs that rigidifies on PAK binding as a bifurcation along the long axis of the molecule does not constitute the binding interface of

any of the partner proteins. This leads to the possibility that the PAK binding redistributes the protein conformational entropy of Cdc42Hs in such a way that the binding surfaces for regulators and effector proteins are made generally more flexible at the expense of the surface of the Cdc42Hs that does not participate in the binding event and rigidifies. Clearly, the dynamical (entropic) aspects of the formation of the various binary and ternary complexes involved in Cdc42 signaling provide potentially rich insights into the regulation of this complex signaling pathway. Such studies are ongoing.

Conclusions

Appropriate measures of changes in internal motion in proteins can provide a foundation for understanding the role of conformational entropy in binding processes and in the transmission of allosteric free energy through a protein matrix [21,26]. For Cdc42Hs, motions of the backbone seem to play only a small role while changes in the internal side-chain motion of the activated Cdc42Hs upon binding the PAK effector protein domain are more pronounced. The change in conformational entropy reported by the picosecond-to-nanosecond dynamics of the methyl axis order parameters on binding the Cdc42Hs·GMPPCP to PBD46 is quantitatively consistent with the empirical calibration of the dynamical proxy "entropy meter" established by calmodulin and catabolite activator protein systems [26]. The contribution of conformational entropy of Cdc42Hs to the overall free energy of complexation with PBD46 is unfavorable with $-T\Delta S_{conf}$ equal to approximately +10 kcal mol^{-1} at 298 K.

The ΔO^2_{axis} values provide the site-specific mapping of the dynamical response to ligand binding. The existence of anisotropic distance-dependent changes in side-chain motion indicates the presence of dynamically mediated allosteric signaling within Cdc42Hs, which could potentially influence subsequent formation of ternary interactions. The duality of the dynamical response in the nucleotide-binding site is consistent with the facilitation of functional events that transpire on binding the PAK domain, that is, the reduced capacity to hydrolyze GTP in the rigidified pocket containing the substrate, and the subsequent exchange of GDP for GTP via facilitated molecular diffusion at the site of increased flexibility sandwiching the guanosine ring. The regions of Cdc42Hs that becomes more flexible upon binding PBD46 contain the Switch II and the GTP-binding pocket as part of the binding interface for all partner structures superimposed: GAP, formin, GDI and GEF. The bifurcation of the dynamic response along the long axis of Cdc42Hs upon binding PAK results in a rigidified surface that does not participate in the binding interface with any of the protein complexes examined. The significance of the apparent redistribution of conformational entropy in Cdc42Hs remains to be fully illuminated and will require examination of ternary complexes to resolve. These studies are ongoing and will be reported elsewhere.

Materials and Methods

Protein preparation

The gene encoding the placental isoform of human Cdc42 (Cdc42Hs isoform 2) was obtained from the American Type Culture Collection (Manassas, VA). Nucleotides corresponding to the first 178 residues (resulting in truncation of the 16-residue unstructured C-terminal tail) were sub-cloned into the cleavable pET15b vector containing the hexa-His-tag (Novagen, Madison, WI) between the NdeI and BamHI restriction sites. This construct was transformed into BL21(DE3)-RIL *Escherichia coli* cells (Stratagene, La Jolla, CA), grown at 37 °C in 1 L cultures using a 1.5× concentration of standard M9 media and induced with 1 mM IPTG (Fisher Scientific, Waltham, MA) at an OD_{600} of ~0.8 for 5 h before harvesting the cells. Protein for most chemical shift assignments was expressed using 1.0 g of ^{15}N-ammonium chloride (Cambridge Isotope Laboratories, Andover, MA) as the sole nitrogen source and $^{13}C_6$-glucose (Cambridge Isotope Laboratories) as the sole carbon source, with the prochirality of methyl groups determined [75] using Cdc42Hs samples grown using 10% ^{13}C-glucose/90% ^{12}C-glucose and 100% $^{15}NH_4Cl$. Protein for nitrogen relaxation experiments was expressed using $^{15}NH_4Cl$ as the sole nitrogen source and unlabeled glucose (Sigma, St. Louis, MO). The pyruvate labeling strategy [40] as modified by Ishima *et al.* was used to prepare protein appropriately labeled for methyl carbon relaxation [33]. Transformed cells were acclimated directly into 99% D_2O-containing M9 media. Expression cultures were grown at 37 °C using $^{15}NH_4Cl$ and unlabeled pyruvate (Sigma) and glucose (Sigma) as the sole nitrogen and carbon sources until an OD_{600} of 0.7 was reached. Specifically labeled carbon sources: 2 g of 3-^{13}C,3,3,3-D_3 (3-position 50–60% D) pyruvate (Isotec, St. Louis, MO) and 200 mg of 4-^{13}C,3,3,4,4,4-D_5 (3-position 97% D, 4-position 50–70% D) 2-ketobutyric acid (Isotec) were then added and shaken at 37 °C for an additional hour. The flasks were then cooled to 30 °C, induced with 1 mM IPTG and grown overnight (16–20 h) before being harvested.

Cdc42Hs was prepared from cells lysed by sonication in 20 mM Tris (pH 7.9), 5 mM imidazole, 0.5 M NaCl, 0.1 mM GDP (Sigma) and ethylenediaminetetraacetic-acid-free protease inhibitor tablets (Roche, Basel, Switzerland). Cell lysate supernatants were loaded onto a column containing Ni^{2+}-NTA superflow resin (Qiagen, Hilden, Germany) and the His-tagged protein was eluted using a linear gradient of imidazole (up to 0.5 M imidazole). This fusion protein was dialyzed into buffer containing 5 mM Tris (pH 7.9), 1.25 mM imidazole and 0.125 M NaCl and was subsequently cleaved at 4 °C with bovine thrombin (Sigma). Cdc42Hs was purified from the cleaved His-tag by Ni^{2+}-NTA column chromatography, pooled, concentrated and exchanged into the nucleotide exchange buffer: 30 mM Tris (pH 8.0), 5 mM $MgCl_2$, 200 mM ammonium sulfate and 0.02% sodium azide.

Purified Cdc42Hs·GDP was exchanged with GMPPCP (Jena Bioscience, Jena, Germany) in the presence of calf intestine alkaline phosphatase agarose beads (Sigma) following a protocol similar to that described by Smith *et al.* [76]. Complete exchange was verified by NMR. Cdc42Hs·GMPPCP was subsequently exchanged into NMR buffer [20 mM imidazole (pH 6.5), 5 mM $MgCl_2$ and 0.04% sodium azide] to remove any remaining GDP, GMP or P_i. Ternary complex samples were made by titrating ^{15}N-labeled PBD46 into appropriately labeled Cdc42Hs·GMPPCP and monitoring the progress using ^{15}N-HSQC NMR experiments. The resulting solution was subsequently concentrated.

The DNA sequence for the 46-residue Cdc42Hs-binding domain of PAK (PBD46) was obtained commercially (Genscript, Piscataway, NJ) and cloned into the cleavable hexa-His/thioredoxin fusion-containing pET32b vector (Novagen) modified to contain a BamHI cleavage site. Expression was performed as described above with $^{15}NH_4Cl$ as the sole nitrogen source and unlabeled glucose as the sole carbon source and, for protein to be used for carbon relaxation experiments, in 95% D_2O media. Soluble PBD46 fusion protein was bound to Ni^{2+}-NTA resin, cleaved from His-tagged thioredoxin with thrombin and repurified over Ni^{2+}-NTA resin in a manner similar to that performed with Cdc42Hs, using buffers in the absence of GDP. No nucleotide exchange step was necessary.

NMR samples

Samples for NMR resonance assignments were concentrated to 1.0 mM Cdc42Hs·GMPPCP (and 1.1 mM ^{15}N-PBD46 where applicable) in buffer containing 20 mM imidazole (pH 6.5), 5 mM $MgCl_2$ (Fisher), 155 μM excess GMPPCP, 20 μM 4,4-dimethyl-4-silapentane-1-sulfonic acid (Sigma) and 0.04% (w/v) sodium azide (Fisher) in either 98% D_2O [for the methyl (H)CCH-TOCSY experiment in the ternary state] or 8% D_2O (for the remainder of experiments). Relaxation samples were concentrated to 0.88 mM Cdc42Hs·GMPPCP (and 1.06 mM ^{15}N-PBD46 where applicable) in the above-mentioned buffer in either 5% (for nitrogen relaxation) or 98% D_2O (for methyl carbon relaxation). The ternary complex was 0.88 mM Cdc42Hs·GMPPCP and 1.06 mM ^{15}N-PBD46 mixed at a ratio of 3:1 for the Cdc42Hs labeled with ^{13}C methyl and ^{15}N amide. The buffer was then 5% D_2O for both methyl carbon and nitrogen relaxation experiments.

NMR spectroscopy

All NMR experiments were collected at 25 °C using Bruker BioSpin Avance III NMR spectrometers equipped with cryogenic probes. Chemical shifts were referenced to 4,4-dimethyl-4-silapentane-1-sulfonic acid [77]. Chemical shift assignment data for both the binary and ternary complexes were collected at 17.6 T. As described above, with two exceptions, chemical shift assignment experiments were collected using uniformly ^{15}N,^{13}C-labeled binary (Cdc42Hs·GMPPCP) or ternary (Cdc42Hs·GMPPCP–PBD46) complexes in NMR buffer containing 8% D_2O. Methyl chirality of both complexes was determined using a 10% ^{13}C-labeled sample [75]. Additionally, the H(C)CH-TOCSY experiment on the ternary complex was performed in buffer containing 98% D_2O.

Standard sequential assignments of backbone resonances [36,78] were obtained from HNCACB and CBCA(CO)NH experiments for the binary complex (and corroborated using published data [5]) and from HNCACB, CBCA(CO)NH and HNCA experiments for the ternary complex (and corroborated using a published ^{15}N-HSQC spectrum [35]). Binary and ternary complex methyl assignments were made using H(C)CH-COSY, H(C)CH-TOCSY [79] and methyl (H)CCH-TOCSY experiments [80], as well as a high-resolution ^{13}C-HSQC on the 10% labeled sample.

Nitrogen relaxation and characterization of macromolecular tumbling

^{15}N-labeled T_1, T_2 and NOE relaxation rates were obtained in both states at 14.1 and 17.6 T using standard methods [36] on a sample containing 0.88 mM ^{15}N-Cdc42Hs·GMPPCP (and 1.06 mM ^{15}N-PBD46 for the ternary complex). Briefly, nine relaxation time points and three duplicate time points were acquired for each of the T_1 and T_2 experiments. Signal intensities, as a function of delay time, were fit to a single-exponential decay function, using a two-parameter or a three-parameter decay function as dictated by a reduced-χ^2 value for the fit. Replicate relaxation time points were used as the error estimate. The estimated errors in relaxation time constants were based upon the covariance matrix of the least square fitting of the exponential decay curves. The heteronuclear steady-state NOE was measured with 5 s of broadband ^{1}H decoupling with the error taken as the baseline RMSD.

All tumbling times and order parameters were fit using an in-house Python scripted relaxation program [81]. Nitrogen model-free fitting routines utilized a grid search approach [82] and employed an effective N–H bond length of 1.04 Å [83] and an ^{15}N CSA tensor breadth of −170 ppm [84]. Only probes not showing a statistically significant contribution of line broadening due to chemical exchange effects (R_{ex}) were used in the determination of global tumbling parameters. The presence of R_{ex} was identified by comparison of reduced-χ^2 values. Internal motion was treated using the model-free spectral density [37]. Errors in O^2 and τ_e parameters are reported as single standard deviation values as estimated via extensive Monte Carlo sampling based on estimated error of the primary relaxation data.

The appropriate tumbling model with corresponding parameters was selected from an isotropic, axially symmetric or anisotropic model [38] using trimmed data sets. Pairwise comparisons in the form of F values were used to determine the appropriate tumbling model:

$$F_x = \frac{E(m)-E(m+x)}{E(m)/(N-m-x)} \quad (1)$$

where m is the number of fitted parameters for the simpler model, x is the number of additional fitted parameters in the higher-order model, N is the total number of probes and $E()$ is

the reduced fitting error of the tumbling model with z, the number of variables, as defined by:

$$E(z) = \frac{\sum_{i=1}^{N}\sum_{j}\left\{\frac{\text{calculated}_j - \text{observed}_v}{\text{meas.error}_j}\right\}^2}{N-z} \quad (2)$$

Improvement is observed via positive F_x values (with $p < 0.05$).

Carbon relaxation and methyl order parameter determination

T_1 and $T_{1\rho}$ ^{13}C relaxation experiments [34] were collected at 14.1 and 17.6 T for both complexes using nine delay points plus three duplicates, as described above for the T_1 and T_2 ^{15}N relaxation experiments. The efficacy of the suppression of methyl R_{ex} by the applied spin-lock was assessed by comparison of relaxation rates obtained using two different RF field strengths [34]. Isotropic tumbling times determined from ^{15}N relaxation data were scaled on the basis of the mole fraction of D_2O to account for the difference in viscosity [85] taking the density of D_2O to be 1.23 times that of H_2O [86,87].

The relaxation rates were considered as the sum of two general components, one arising from local interactions with bonded nuclei and another one arising from interactions with remote nuclei with a given statistical occupancy [33,34]:

$$\frac{1}{T_i^{\text{obs}}} = R_i^{\text{obs}} = \left(R_i^{\text{CH}} + 2R_i^{\text{CD}}\right) + \sum R_i^{\text{CX}} \quad (3)$$

where the observed methyl ^{13}C longitudinal (R_1^{obs}) or transverse (R_2^{obs}) relaxation rate is considered in the context of the $^{13}C^1H^2D_2$ isotopomer surrounded by non-bonded remote spins of a given nuclear type having a projected occupancy for the isotopic enrichment. The structures of the binary and ternary complexes of Cdc42Hs were used to determine an effective distance ($r_{\text{eff}}^{\text{CX}}$) corresponding to the summed dipole–dipole interactions for all remote X spin interactions to a methyl ^{13}C, where $r_{\text{eff}}^{\text{CX}} = (\sum f_X r_{\text{CX}}^{-6})^{-1/6}$. Residual ^{1}H and ^{13}C at non-methyl sites was estimated to be <5% and ^{15}N enrichment was taken as 100%. Other nuclear types were evaluated at natural abundance. Standard equations for the dipole–dipole and CSA relaxation mechanisms were utilized and the model-free spectral density was employed [37].

Determination of carbon methyl model-free parameters [37] from the carbon relaxation data employed standard equations for the dipole–dipole and CSA relaxation mechanisms, a grid search approach using methyl-type-specific CSA tensor breadth values [88] (Ala C^β = 18 ppm, Val C^γ = 23.25 ppm, Leu C^δ = 30 ppm, Ile $C^{\gamma 2}$ = 21.25 ppm, Ile $C^{\delta 1}$ = 17.5 ppm, Thr $C^{\gamma 2}$ = 24.5 ppm, Met C^ε = 18.5 ppm), standard methyl geometries (including ^{13}C–^{1}H and ^{13}C–^{2}H bond lengths of 1.115 Å) and the isotropic tumbling parameters determined by analysis of ^{15}N relaxation (see above). The squared generalized order parameter (O^2) and the internal correlation time (τ_e) were determined for each carbon methyl probe. The reported squared generalized order parameters for the motion of the methyl carbon symmetry axis (O^2_{axis}) are equal to O^2/0.111.

Structural and additional analysis

Gaussian curves were fitted using KaleidaGraph (Synergy Software, Reading, PA). Molecular representations were rendered using the PyMOL molecular visualization system (Schrödinger, Portland, OR) [89]. Definition of regions of Cdc42Hs having dynamical changes upon PBD46 binding was determined by extrapolating the sign of change of the closest determined probe to each atom in Cdc42Hs using an in-house script and model 1 of the NMR-based structure (PDB ID: 1EES) [14]. Distances of probes to the PBD46 peptide were also calculated using model 1 of 1EES [14]. Intermolecular distances reported are those from the probe carbon to the nearest non-proton atom of PBD46. The align function of PyMOL [89] was used to structurally align the Cdc42 components of Cdc42·PBD46 (PDB ID: 1EES [14]), Cdc42·mDia formin (PDB ID: 3EG5 [61]), Cdc42·Dbs GEF (PDB ID: 1KZG [74]) and Cdc42·Cdc42GAP (PDB ID: 1GRN [56]) for analysis of potential three-protein interactions.

The contribution of solvent to the binding entropy was calculated from the change in polar and nonpolar surface area upon binding. The CCP4 package was used to calculate ASAs [53] of Cdc42Hs and PBD46 in the ternary state based on the structure determined by Gizachew *et al.* (1EES) [14] and Cdc42Hs in the binary state based on the structure by Phillips *et al.* (2QRZ) [54]. The PBD46 structure in the free state was modeled by maintaining the single helix at residues 37–42 with the remainder of the protein in an extended conformation. The solvent entropy was calculated from the change in polar and nonpolar ASA using the parameters of Gomez *et al.* [90].

The iterative interquartile range method [45] was used to identify sites with unusually large changes that fall outside a simple Gaussian distribution of O^2_{axis}. Briefly, order parameter changes falling 1.5 times or more outside the interquartile (i.e., the middle 25–75%) range were identified and removed.

Accession numbers

Chemical shift assignments and order parameters for backbone and methyl probes are deposited to the BMRB under accession numbers 18251 (Cdc42Hs·GMPPCP) and 18252 (Cdc42Hs·GMPPCP·PBD46).

Acknowledgements

This work is supported by National Institutes of Health grant GM102447. J.D. acknowledges financial support from the Wenner-Gren Foundations.

Appendix A. Supplementary data

Supplementary data to this article can be found online at http://dx.doi.org/10.1016/j.jmb.2014.07.031.

Received 7 June 2014;
Received in revised form 29 July 2014;
Accepted 31 July 2014
Available online 7 August 2014

Keywords:
carbon methyl relaxation;
pico-nanosecond dynamics;
NMR-derived order parameters;
distance-dependent dynamical allostery

[1]Present address: V. R. Moorman, Department of Chemistry and Biochemistry, Kettering University, 1700 University Avenue, Flint, MI 48504, USA.

Abbreviations used:
ASA, accessible surface area; CRIB, Cdc42/Rac interactive binding; CSA, chemical shift anisotropy; GAP, GTPase-activating protein; GDI, guanine nucleotide dissociation inhibitor; GDP, guanosine diphosphate; GEF, guanine nucleotide exchange factor; GTP, guanosine triphosphate; GTPase, guanosine triphosphatase; HSQC, heteronuclear single quantum coherence; NOE, nuclear Overhauser enhancement; PAK3, p21-activated kinase 3; TOCSY, total correlated spectroscopy; ITC, isothermal titration calorimetry; BMRB, Biological Magnetic Resonance Bank.

References

[1] Cerione RA. Cdc42: new roads to travel. Trends Cell Biol 2004;14:127–32.
[2] Fededa JP, Gerlich DW. Molecular control of animal cell cytokinesis. Nat Cell Biol 2012;14:440–7.
[3] Cherfils J, Zeghouf M. Regulation of small GTPases by GEFs, GAPs, and GDIs. Physiol Rev 2013;93:269–309.
[4] Hakoshima T, Shimizu T, Maesaki R. Structural basis of the Rho GTPase signaling. J Biochem 2003;134:327–31.
[5] Feltham JL, Dotsch V, Raza S, Manor D, Cerione RA, Sutcliffe MJ, et al. Definition of the switch surface in the solution structure of Cdc42Hs. Biochemistry 1997;36:8755–66.
[6] Ke Y, Lei M, Solaro RJ. Regulation of cardiac excitation and contraction by p21 activated kinase-1. Prog Biophys Mol Biol 2008;98:238–50.
[7] Dummler B, Ohshiro K, Kumar R, Field J. Pak protein kinases and their role in cancer. Cancer Metastasis Rev 2009;28:51–63.
[8] Szczepanowska J. Involvement of Rac/Cdc42/PAK pathway in cytoskeletal rearrangements. Acta Biochim Pol 2009;56:225–34.
[9] Cotteret S, Chernoff J. The evolutionary history of effectors downstream of Cdc42 and Rac. Genome Biol 2002;3:1–8.
[10] Manser E, Leung T, Salihuddin H, Zhao ZS, Lim L. A brain serine/threonine protein kinase activated by Cdc42 and Rac1. Nature 1994;367:40–6.
[11] Wennerberg K, Der CJ. Rho-family GTPases: it's not only Rac and Rho (and I like it). J Cell Sci 2004;117:1301–12.
[12] Dorjgotov D, Jurca ME, Fodor-Dunai C, Szucs A, Otvos K, Klement E, et al. Plant Rho-type (Rop) GTPase-dependent activation of receptor-like cytoplasmic kinases *in vitro*. FEBS Lett 2009;583:1175–82.
[13] Abramovitz A, Gutman M, Nachliel E. Structural coupling between the Rho-insert domain of Cdc42 and the geranylgeranyl binding site of RhoGDI. Biochemistry 2012;51:715–23.
[14] Gizachew D, Guo W, Chohan KK, Sutcliffe MJ, Oswald RE. Structure of the complex of Cdc42Hs with a peptide derived from P-21 activated kinase. Biochemistry 2000;39:3963–71.
[15] Stevens WK, Vranken W, Goudreau N, Xiang H, Xu P, Ni F. Conformation of a Cdc42/Rac interactive binding peptide in complex with Cdc42 and analysis of the binding interface. Biochemistry 1999;38:5968–75.
[16] Wodak SJ, Janin J. Structural basis of macromolecular recognition. Adv Protein Chem 2002;61:9–73.
[17] Gilson MK, Zhou HX. Calculation of protein–ligand binding affinities. Annu Rev Biophys Biomol Struct 2007;36:21–42.
[18] Cooper A. Thermodynamic fluctuations in protein molecules. Proc Natl Acad Sci USA 1976;73:2740–1.
[19] Cooper A, Dryden DTF. Allostery without conformational change—a plausible model. Eur Biophys J 1984;11:103–9.
[20] Karplus M, Ichiye T, Pettitt BM. Configurational entropy of native proteins. Biophys J 1987;52:1083–5.
[21] Wand AJ. On the dynamic origins of allosteric activation. Science 2001;293:1395.
[22] Wand AJ. The dark energy of proteins comes to light: conformational entropy and its role in protein function revealed by NMR relaxation. Curr Opin Struct Biol 2013;23:75–81.
[23] Igumenova TI, Frederick KK, Wand AJ. Characterization of the fast dynamics of protein amino acid side chains using NMR relaxation in solution. Chem Rev 2006;106:1672–99.
[24] Frederick KK, Marlow MS, Valentine KG, Wand AJ. Conformational entropy in molecular recognition by proteins. Nature 2007;448:325–9.
[25] Marlow MS, Dogan J, Frederick KK, Valentine KG, Wand AJ. The role of conformational entropy in molecular recognition by calmodulin. Nat Chem Biol 2010;6:352–8.
[26] Kasinath V, Sharp KA, Wand AJ. Microscopic insights into the NMR relaxation-based protein conformational entropy meter. J Am Chem Soc 2013;135:15092–100.
[27] Lee AL, Kinnear SA, Wand AJ. Redistribution and loss of side chain entropy upon formation of a calmodulin-peptide complex. Nat Struct Biol 2000;7:72–7.
[28] Li Z, Raychaudhuri S, Wand AJ. Insights into the local residual entropy of proteins provided by NMR relaxation. Protein Sci 1996;5:2647–50.
[29] Yap KL, Kim J, Truong K, Sherman M, Yuan T, Ikura M. Calmodulin target database. J Struct Funct Genomics 2000;1:8–14.
[30] Der CJ. RAS family GTPases. Proteins and cell regulation, 4. Dordrecht: Springer; 2006.
[31] Loh AP, Guo W, Nicholson LK, Oswald RE. Backbone dynamics of inactive, active, and effector-bound Cdc42Hs from measurements of ^{15}N relaxation parameters at multiple field strengths. Biochemistry 1999;38:12547–57.
[32] Loh AP, Pawley N, Nicholson LK, Oswald RE. An increase in side chain entropy facilitates effector binding: NMR characterization of the side chain methyl group dynamics in Cdc42Hs. Biochemistry 2001;40:4590–600.
[33] Ishima R, Louis JM, Torchia DA. Optimized labeling of $^{13}CHD_2$ methyl isotopomers in perdeuterated proteins: potential advantages for ^{13}C relaxation studies of methyl dynamics of larger proteins. J Biomol NMR 2001;21:167–71.

[34] Tugarinov V, Kay LE. Quantitative ^{13}C and ^{2}H NMR relaxation studies of the 723-residue enzyme malate synthase G reveal a dynamic binding interface. Biochemistry 2005;44:15970–7.
[35] Guo W, Sutcliffe MJ, Cerione RA, Oswald RE. Identification of the binding surface on Cdc42Hs for p21-activated kinase. Biochemistry 1998;37:14030–7.
[36] Farrow NA, Muhandiram R, Singer AU, Pascal SM, Kay CM, Gish G, et al. Backbone dynamics of a free and phosphopeptide-complexed Src homology 2 domain studied by ^{15}N NMR relaxation. Biochemistry 1994;33:5984–6003.
[37] Lipari G, Szabo A. Model-free approach to the interpretation of nuclear magnetic-resonance relaxation in macromolecules 1. Theory and range of validity. J Am Chem Soc 1982;104:4546–59.
[38] Tjandra N, Feller SE, Pastor RW, Bax A. Rotational diffusion anisotropy of human ubiquitin from ^{15}N NMR relaxation. J Am Chem Soc 1995;117:12562–6.
[39] Jarymowycz VA, Stone MJ. Fast time scale dynamics of protein backbones: NMR relaxation methods, applications, and functional consequences. Chem Rev 2006;106:1624–71.
[40] Lee AL, Urbauer JL, Wand AJ. Improved labeling strategy for ^{13}C relaxation measurements of methyl groups in proteins. J Biomol NMR 1997;9:437–40.
[41] Muhandiram DR, Yamazaki T, Sykes BD, Kay LE. Measurement of ^{2}H T_1 and $T_{1\rho}$ relaxation-times in uniformly ^{13}C-labeled and fractionally ^{2}H-labeled proteins in solution. J Am Chem Soc 1995;117:11536–44.
[42] Millet O, Muhandiram DR, Skrynnikov NR, Kay LE. Deuterium spin probes of side-chain dynamics in proteins. 1. Measurement of five relaxation rates per deuteron in ^{13}C-labeled and fractionally ^{2}H-enriched proteins in solution. J Am Chem Soc 2002;124:6439–48.
[43] Ishima R, Petkova AP, Louis JM, Torchia DA. Comparison of methyl rotation axis order parameters derived from model-free analyses of ^{2}H and ^{13}C longitudinal and transverse relaxation rates measured in the same protein sample. J Am Chem Soc 2001;123:6164–71.
[44] Sharp KA, Kasinath V, Wand AJ. Banding of NMR-derived methyl order parameters: implications for protein dynamics. Proteins 2014. http://dx.doi.org/10.1002/prot.24566 [in press].
[45] Moore DS, McCabe GP. Introduction to the practice of statistics. 2nd ed. New York: Freeman; 1993.
[46] Schreiber G, Fersht AR. Energetics of protein–protein interactions: analysis of the barnase-barstar interface by single mutations and double mutant cycles. J Mol Biol 1995;248:478–86.
[47] Fodor AA, Aldrich RW. On evolutionary conservation of thermodynamic coupling in proteins. J Biol Chem 2004;279:19046–50.
[48] Chi CN, Elfstrom L, Shi Y, Snall T, Engstrom A, Jemth P. Reassessing a sparse energetic network within a single protein domain. Proc Natl Acad Sci USA 2008;105:4679–84.
[49] Li DW, Meng D, Bruschweiler R. Short-range coherence of internal protein dynamics revealed by high-precision *in silico* study. J Am Chem Soc 2009;131:14610–1.
[50] Tzeng S-R, Kalodimos C. Protein activity regulation by conformational entropy. Nature 2012;488:236–40.
[51] Guo, W. (1999). Ph.D. Thesis, Cornell University.
[52] D'Aquino JA, Gomez J, Hilser VJ, Lee KH, Amzel LM, Freire E. The magnitude of the backbone conformational entropy change in protein folding. Proteins 1996;25:143–56.
[53] Bailey S. The CCP4 suite: programs for protein crystallography. Acta Crystallogr Sect D Biol Crystallogr 1994;50:760–3.
[54] Phillips MJ, Calero G, Chan B, Ramachandran S, Cerione RA. Effector proteins exert an important influence on the signaling-active state of the small GTPase Cdc42. J Biol Chem 2008;283:14153–64.
[55] Morreale A, Venkatesan M, Mott HR, Owen D, Nietlispach D, Lowe PN, et al. Structure of Cdc42 bound to the GTPase binding domain of PAK. Nat Struct Biol 2000;7:384–8.
[56] Nassar N, Hoffman GR, Manor D, Clardy JC, Cerione RA. Structures of Cdc42 bound to the active and catalytically compromised forms of Cdc42GAP. Nat Struct Biol 1998;5:1047–52.
[57] Kamerlin SC, Sharma PK, Prasad RB, Warshel A. Why nature really chose phosphate. Q Rev Biophys 2013;46:1–132.
[58] Klahn M, Rosta E, Warshel A. On the mechanism of hydrolysis of phosphate monoesters dianions in solutions and proteins. J Am Chem Soc 2006;128:15310–23.
[59] Shuker SB, Hajduk PJ, Meadows RP, Fesik SW. Discovering high-affinity ligands for proteins: SAR by NMR. Science 1996;274:1531–4.
[60] Motlagh HN, Wrabl JO, Li J, Hilser VJ. The ensemble nature of allostery. Nature 2014;508:331–9.
[61] Lammers M, Meyer S, Kuhlmann D, Wittinghofer A. Specificity of interactions between mDia isoforms and Rho proteins. J Biol Chem 2008;283:35236–46.
[62] Murai KK, Pasquale EB. 'Eph'ective signaling: forward, reverse and crosstalk. J Cell Sci 2003;116:2823–32.
[63] Buchsbaum RJ, Connolly BA, Feig LA. Interaction of Rac exchange factors Tiam1 and Ras-GRF1 with a scaffold for the p38 mitogen-activated protein kinase cascade. Mol Cell Biol 2002;22:4073–85.
[64] Mertens AE, Roovers RC, Collard JG. Regulation of Tiam1-Rac signalling. FEBS Lett 2003;546:11–6.
[65] Rossman KL, Der CJ, Sondek J. GEF means go: turning on RHO GTPases with guanine nucleotide-exchange factors. Nat Rev Mol Cell Biol 2005;6:167–80.
[66] Lechler T, Jonsdottir GA, Klee SK, Pellman D, Li R. A two-tiered mechanism by which Cdc42 controls the localization and activation of an Arp2/3-activating motor complex in yeast. J Cell Biol 2001;155:261–70.
[67] Johnson DI. Cdc42: an essential Rho-type GTPase controlling eukaryotic cell polarity. Microbiol Mol Biol Rev 1999;63:54–105.
[68] Wang L, Zhu K, Zheng Y. Oncogenic Dbl, Cdc42, and p21-activated kinase form a ternary signaling intermediate through the minimum interactive domains. Biochemistry 2004;43:14584–93.
[69] Sinha S, Yang W. Cellular signaling for activation of Rho GTPase Cdc42. Cell Signalling 2008;20:1927–34.
[70] Vetter IR, Wittinghofer A. The guanine nucleotide-binding switch in three dimensions. Science 2001;294:1299–304.
[71] Wittinghofer A, Vetter IR. Structure-function relationships of the G domain, a canonical switch motif. Annu Rev Biochem 2011;80:943–71.
[72] Prasad BR, Plotnikov NV, Lameira J, Warshel A. Quantitative exploration of the molecular origin of the activation of GTPase. Proc Natl Acad Sci USA 2013;110:20509–14.
[73] Hoffman GR, Nassar N, Cerione RA. Structure of the Rho family GTP-binding protein Cdc42 in complex with the multifunctional regulator RhoGDI. Cell 2000;100:345–56.
[74] Rossman KL, Worthylake DK, Snyder JT, Siderovski DP, Campbell SL, Sondek J. A crystallographic view of interactions between Dbs and Cdc42: PH domain-assisted guanine nucleotide exchange. EMBO J 2002;21:1315–26.
[75] Neri D, Szyperski T, Otting G, Senn H, Wuthrich K. Stereospecific nuclear magnetic resonance assignments of

the methyl groups of valine and leucine in the DNA-binding domain of the 434 repressor by biosynthetically directed fractional ^{13}C labeling. Biochemistry 1989;28:7510–6.

[76] Smith SJ, Rittinger K. Preparation of GTPases for structural and biophysical analysis. Methods Mol Biol 2002;189:13–24.

[77] Markley JL, Bax A, Arata Y, Hilbers CW, Kaptein R, Sykes BD, et al. Recommendations for the presentation of NMR structures of proteins and nucleic acids—IUPAC-IUBMB-IUPAB Inter-Union Task Group on the standardization of data bases of protein and nucleic acid structures determined by NMR spectroscopy. Eur J Biochem 1998;256:1–15.

[78] Sattler M, Schleucher J, Griesinger C. Heteronuclear multidimensional NMR experiments for the structure determination of proteins in solution employing pulsed field gradients. Prog Nucl Magn Reson Spectrosc 1999;34: 93–158.

[79] Kay LE, Xu GY, Singer AU, Muhandiram DR, Formankay JD. A gradient-enhanced HCCH TOCSY experiment for recording side-chain ^{1}H and ^{13}C correlations in H_2O samples of proteins. J Magn Reson Ser B 1993;101:333–7.

[80] Uhrin D, Uhrinova S, Leadbeater C, Nairn J, Price NC, Barlow PN. 3D $HCCH_3$-TOCSY for resonance assignment of methyl-containing side chains in ^{13}C-labeled proteins. J Magn Reson 2000;142:288–93.

[81] Kasinath V, Valentine KG, Wand AJ. A 13C labeling strategy reveals a range of aromatic side chain motion in calmodulin. J Am Chem Soc 2013;135:9560–3.

[82] Dellwo MJ, Wand AJ. Model-independent and model-dependent analysis of the global and internal dynamics of cyclosporine-A. J Am Chem Soc 1989;111:4571–8.

[83] Ottiger M, Bax A. Determination of relative $N\text{-}H^N$ N-C′, C^α-C′, and $C^\alpha\text{-}H^\alpha$ effective bond lengths in a protein by NMR in a dilute liquid crystalline phase. J Am Chem Soc 1998;120: 12334–41.

[84] Tjandra N, Grzesiek S, Bax A. Magnetic field dependence of nitrogen-proton J splittings in ^{15}N-enriched human ubiquitin resulting from relaxation interference and residual dipolar coupling. J Am Chem Soc 1996;118:6264–72.

[85] Kestin J, Imaishi N, Nott SH, Nieuwoudt JC, Sengers JV. Viscosity of light and heavy-water and their mixtures. Phys A 1985;134:38–58.

[86] Baker WN. A new comparison of the viscosity of D_2O with that of H_2O. J Chem Phys 1936;4:294–5.

[87] Harris KR, Woolf LA. Temperature and volume dependence of the viscosity of water and heavy water at low temperatures. J Chem Eng Data 2004;49:1064–9.

[88] Ye C, Fu R, Hu J, Hou L, Ding S. Carbon-13 chemical shift anisotropies of solid amino acids. Magn Reson Chem 1993; 31:699–704.

[89] DeLano WL. The PyMOL molecular graphics system. San Carlos, CA: DeLano Scientific; 2002.

[90] Gomez J, Hilser VJ, Xie D, Freire E. The heat capacity of proteins. Proteins 1995;22:404–12.